Article

# Investigation of Solvent Effects for the Claisen Rearrangement of Chorismate to Prephenate: Mechanistic Interpretation via Near Attack Conformations

Matthew P. Repasky, Cristiano Ruch Werneck Guimares, Jayaraman Chandrasekhar, Julian Tirado-Rives, and William L. Jorgensen

*J. Am. Chem. Soc.*, **2003**, 125 (22), 6663-6672• DOI: 10.1021/ja021423z • Publication Date (Web): 08 May 2003



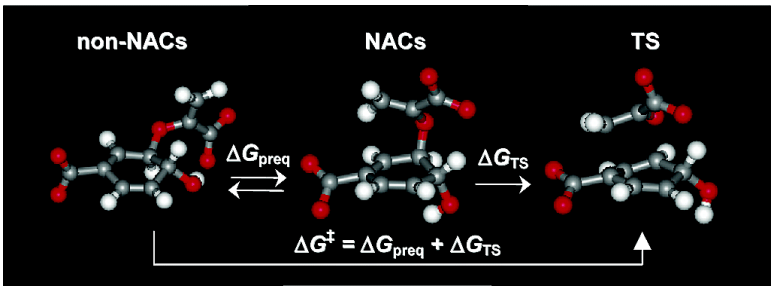


## More About This Article

Additional resources and features associated with this article are available within the HTML version:

- Supporting Information
- Links to the 3 articles that cite this article, as of the time of this article download
- Access to high resolution figures
- Links to articles and content related to this article
- Copyright permission to reproduce figures and/or text from this article

View the Full Text HTML

J|A|C|S
ARTICLES
Published on Web 05/08/2003

# Investigation of Solvent Effects for the Claisen Rearrangement of Chorismate to Prephenate: Mechanistic Interpretation via Near Attack Conformations

Matthew P. Repasky,† Cristiano Ruch Werneck Guimarães, Jayaraman Chandrasekhar,‡ Julian Tirado-Rives, and William L. Jorgensen*

*Contribution from the Department of Chemistry, Yale University, 225 Prospect Street, New Haven, Connecticut 06520-8107*

Received December 9, 2002; E-mail: william.jorgensen@yale.edu

***Abstract:*** Solvent effects on the rate of the Claisen rearrangement of chorismate to prephenate have been examined in water and methanol. The preequilibrium free-energy differences between diaxial and diequatorial conformers of chorismate, which had previously been implicated as the sole basis for the observed 100-fold rate increase in water over methanol, have been reframed using the near attack conformation (NAC) concept of Bruice and co-workers. Using a combined QM/MM Monte Carlo/free-energy perturbation (MC/FEP) method, 82%, 57%, and 1% of chorismate conformers were found to be NAC structures (NACs) in water, methanol, and the gas phase, respectively. As a consequence, the conversion of non-NACs to NACs provides no free-energy contributions to the overall relative reaction rates in water versus methanol. Free-energy perturbation calculations yielded differences in free energies of activation for the two polar protic solvents and the gas phase. The rate enhancement in water over the gas phase arises from preferential hydration of the transition state (TS) relative to the reactants via increased hydrogen bonding and long-range electrostatic interactions, which accompany bringing the two negatively charged carboxylates into closer proximity. More specifically, there is an increase of 1.3 and 0.6 hydrogen bonds to the carboxylate groups and the ether oxygen, respectively, in going from the reactant to the TS in water. In methanol, the corresponding changes in hydrogen bonding with first shell solvent molecules are small; the rate enhancement arises primarily from the enhanced long-range interactions with solvent molecules. Thus, the reaction occurs faster in water than in methanol due to greater stabilization of the TS in water by specific interactions with first shell solvent molecules.

## Introduction

The Claisen rearrangement of chorismate to prephenate is a key reaction along the Shikimate pathway for generating aromatic amino acids in plant, fungal, and bacterial systems.[1−3] The reaction is a relatively rare example of a chemical transformation that occurs via an identical mechanism in various solvents as well as within the enzymatic environment provided by chorismate mutase. This fact well positions the chorismate to prephenate rearrangement to further our understanding of general mechanisms of enzymatic catalysis, where detailed thermodynamic information must be obtained within both the enzymatic and the aqueous environments. The rearrangement has been postulated to occur as shown in Scheme 1. An initial preequilibrium between the inactive pseudodiequatorial and active pseudodiaxial conformers of chorismate precedes conversion of the pseudodiaxial conformer to prephenate via a concerted asynchronous transition state. By NMR[4] and theoretical studies,[5] it has been suggested that the 100-fold rate enhancement of the Claisen rearrangement in going from

***Scheme 1.*** The Chorismate to Prephenate Rearrangement

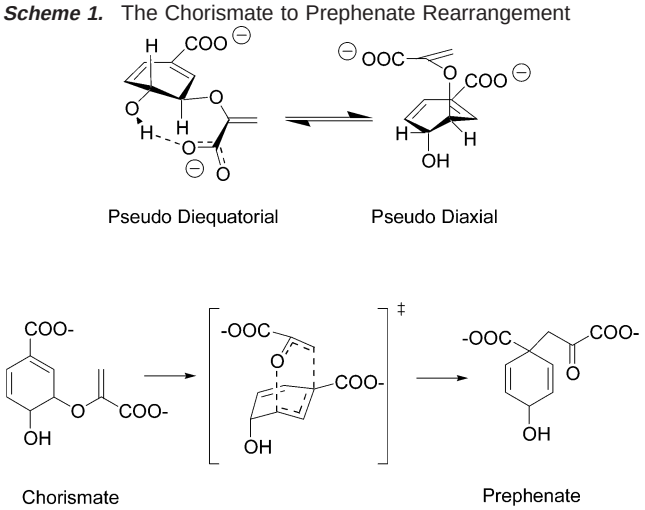


† Current address: Schrödinger Inc., 120 West Forty-Fifth Street, New York, NY 10036.

‡ Current address: Neurogen Corp., 35 Northeast Industrial Rd., Branford, CT 06405.

(1) Ganem, B. *Angew. Chem., Int. Ed. Engl.* **1996**, *35*, 936−945.
(2) Haslam, E. *Shikimic Acid: Metabolism and Metabolites*; John Wiley & Sons: New York, 1993.
(3) Conn, E. E. In *The Shikimic Acid Pathway*; Conn, E. E., Ed.; Recent Advances in Phytochemistry; Plenum Press: New York, 1986.
(4) Copley, S. D.; Knowles, J. R. *J. Am. Chem. Soc.* **1987**, *109*, 5008−5013.

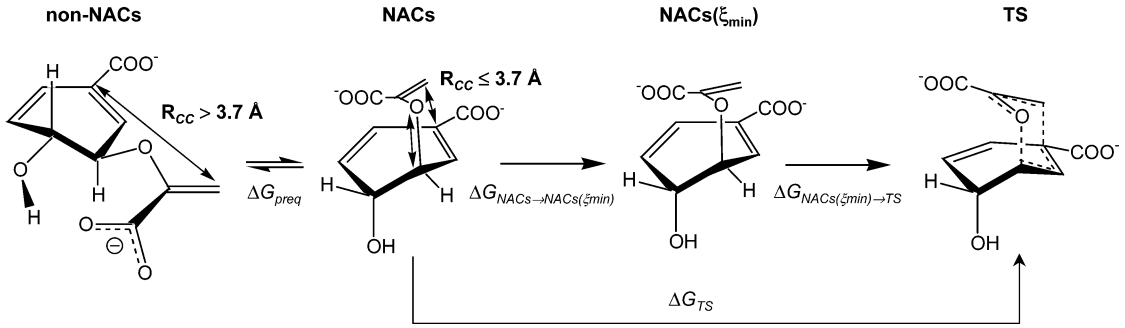


***Figure 1.*** Important steps in the NAC-based model for the chorismate to prephenate rearrangement. Chorismate conformers with $R_{CC} \leq 3.7$ Å are considered as NACs.

methanol to water arises primarily from a change in the conformer populations in the preequilibrium step, estimated to account for about one-half of the total by NMR and all of the rate enhancement theoretically.

An alternative framework for the analysis of enzymatic reactions has been provided by Bruice and co-workers with the near attack conformation (NAC) concept.[6−10] This concept has also been used by other authors.[11,12] NAC structures (NACs) possess the proper geometric juxtaposition of groups for a reaction to proceed directly to a transition state (TS) without significant bond stretching/contraction, angle bending, or torsional motion. In the previous work examining solvent effects on the Claisen rearrangement of chorismate to prephenate, pseudodiaxial and pseudodiequatorial conformers were treated effectively as NACs and non-NACs, respectively.[5] However, all pseudodiaxial conformers, that is, those with the hydroxyl and enol pyruvate groups in axial configurations, are not necessarily NACs. For instance, simple rotation about the ether oxygen to ring carbon bond can lead to a number of conformers which, while being pseudodiaxial, are most decidedly not NACs. Also, due to the flatness of the six-membered ring, a number of pseudodiequatorial conformers have sufficiently small forming C−C distances to be NACs. In a molecular dynamics study of the catalyzed reaction, Hur and Bruice have classified NACs for the chorismate rearrangement using geometrical criteria such that NACs are required to have distances less than 3.70 Å for the forming C−C bond and an attacking angle below 40°.[8] As pointed by Shurki et al.,[13] although the NAC framework is a quantitative concept, the way the parameters (distance/angle) are chosen is somewhat arbitrary. However, as a more general and less restrictive definition of a reactive conformer, the non-NACs/NACs equilibrium can be argued to have greater relevance for the chorismate to prephenate reaction mechanism than consideration of the pseudodiequatorial/pseudodiaxial equilibrium as a prestep. To clarify the contribution of the preequilibrium process to the overall activation barrier, we have reexamined solvent effects on the Claisen rearrangement of chorismate to prephenate in the gas phase, methanol, and water, employing the NAC concept. The computational approach that is developed is a general one that can be applied to the NAC-based analysis of other reactions.

**NAC-Based Model for the Chorismate to Prephenate Rearrangement.** For a unimolecular reaction such as the Claisen rearrangement, $\Delta G^{\ddagger}$ either in solution or in the gas phase can be divided into two components (Figure 1). The first component, the preequilibrium free energy ($\Delta G_{\text{preq}}$), is the free energy associated with the process of orienting chorismate in appropriate conformations, NACs, that are well juxtaposed to lead directly to the TS of the reaction. Ground-state conformations that are not properly aligned for reaction are called non-NACs and are differentiated from NACs following some geometry-based criterion. Because non-NACs are in equilibrium with NACs, $\Delta G_{\text{preq}}$ can be estimated by counting the number of NACs and non-NACs sampled in molecular dynamics or Monte Carlo simulations using the following equation:

$$\Delta G_{\text{preq}} = -RT \ln \frac{P_{\text{NACs}}}{P_{\text{non-NACs}}} \qquad (1)$$

In eq 1, $P_{\text{NACs}}$ and $P_{\text{non-NACs}}$ are the probabilities of sampling NACs and non-NACs, respectively. Alternatively, $\Delta G_{\text{preq}}$ can be estimated by obtaining a potential of mean force (pmf)[14] curve for the reaction coordinate that converts non-NACs into NACs. $P_{\text{NACs}}$ and $P_{\text{non-NACs}}$ may then be derived from the pmf. If the number of non-NACs is greater than the number of NACs, $\Delta G_{\text{preq}}$ will be positive. Consequently, $\Delta G^{\ddagger}$ must include contributions from $\Delta G_{\text{preq}}$.

It is important to note that NACs are a collection of structures with different geometries for the reaction coordinate that generates the TS ($\xi$, e.g., the difference in the lengths of the forming C−C and breaking C−O bonds), and only a subset of NACs displays the free-energy minimum geometry for this reaction coordinate (NACs($\xi_{\text{min}}$)). Pmf calculations can be performed to follow a reaction coordinate from a particular reference geometry yielding free-energy barriers for reactions. To facilitate the pmf calculations, we assume that all NACs must converge to NACs($\xi_{\text{min}}$) prior to proceeding to the TS. Therefore, the second component of $\Delta G^{\ddagger}$, the free energy associated with the conversion of NACs into TS ($\Delta G_{\text{TS}}$), is broken into two quantities. The first, the free energy associated with the conversion of all NACs into NACs($\xi_{\text{min}}$), can be

(5) Carlson, H. A.; Jorgensen, W. L. *J. Am. Chem. Soc.* **1996**, *118*, 8475−8484.
(6) Lightstone, F. C.; Bruice, T. C. *J. Am. Chem. Soc.* **1996**, *118*, 2595−2605.
(7) Torres, R.; Bruice, T. C. *Proc. Natl. Acad. Sci. U.S.A.* **1998**, *95*, 11077−11082.
(8) Hur, S.; Bruice, T. C. *Proc. Natl. Acad. Sci. U.S.A.* **2002**, *99*, 1176−1181.
(9) Bruice, T. C.; Lightstone, F. C. *Acc. Chem. Res.* **1999**, *32*, 127−136.
(10) Torres, R.; Bruice, T. C. *J. Am. Chem. Soc.* **2000**, *122*, 781−791.
(11) Kollman, P. A.; Kuhn, B.; Perakyla, M. *J. Phys. Chem. B* **2002**, *106*, 1537−1542.
(12) Shrimpton, P.; Allemann, R. K. *Protein Sci.* **2002**, *11*, 1442−1451.
(13) Shurki, A.; Štrajbl, M.; Villà, J.; Warshel, A. *J. Am. Chem. Soc.* **2001**, *123*, 4097−4107.
(14) Beveridge, D. L.; DiCapua, F. M. *Annu. Rev. Biophys. Biophys. Chem.* **1989**, *18*, 431−492.

calculated by the following equation:

$$\Delta G_{\mathrm{NACs}\rightarrow\mathrm{NACs}(\xi\mathrm{min})} = -RT \ln P_{\mathrm{NACs}(\xi\mathrm{min})} \qquad (2)$$

In eq 2, $P_{\mathrm{NACs}(\xi\mathrm{min})}$ is the probability of sampling the subset NACs($\xi_{\mathrm{min}}$) from the entire population of NACs. The second, obtained by a pmf calculation, is the free energy associated with the conversion of NACs($\xi_{\mathrm{min}}$) into the TS for the reaction. Thus, the chorismate to prephenate rearrangement in solution can be faster than the reaction in the gas phase by increasing the number of NACs and/or by solvating the TS more favorably than the NACs.

## Computational Details

The first step is to examine the reaction in the gas phase and obtain the minimum energy reaction path (MERP). This was done in a manner similar to that previously applied to investigate solvent effects on Diels−Alder reactions,[15,16] 1,3-dipolar cycloadditions,[17] and Claisen[18] and Mislow−Evans[19] rearrangements. Characterization of the stationary points on the reaction path, including chorismate, prephenate, and the TS, was performed here using the AM1[20] Hamiltonian, as implemented in MOPAC 6.0.[21] The transition state was identified as having a single negative eigenvalue, corresponding to the appropriate bond forming/breaking mechanism. Taking the transition state structure as the initial geometry for application of the intrinsic reaction coordinate (IRC) following algorithm,[22] a series of structures were identified along a reaction path denoted by the forming C−C and breaking C−O bonds. Terminal structures of the IRC were then linearly coupled to the potential energy minimum structures for chorismate and prephenate. Maintaining individual structures with an average difference between the C−O and C−C bonds of approximately 0.15 Å, we found that this procedure generated a reaction path with 39 structures.

Free-energy changes in the gas phase, methanol, and water were obtained from the gas-phase MERP via Monte Carlo (MC) statistical mechanics in conjunction with free-energy perturbation (FEP) calculations using double-wide sampling. However, as an advance over previous studies of solvent effects using MERPs, with the exception of the reaction coordinate itself ($\xi$, the difference in the lengths of the forming C−C and breaking C−O bonds), the remainder of the system is fully flexible in all calculations. Such sampling is only practical at this time using a semiempirical quantum mechanics method. In water and in the gas phase, no intermediate state was used to perturb between adjacent MERP $\xi$ values. However, larger free-energy fluctuations occurred in methanol and necessitated using one intermediate state to perturb between adjacent $\xi$ values. Thus, a total of 19 MC simulations were performed in water and the gas phase to obtain the one-dimensional (1D) pmf curve, while in methanol a total of 38 MC simulations were required.

Starting from the 1D pmf curves, we then located the true critical points on the free-energy surfaces by exploring the regions surrounding the free-energy minimum and maximum in the gas phase and in the two solvents. Starting with the gas-phase geometry for $\xi$ at the potential energy minimum for chorismate, we generated eight perturbed states by adjusting the two degrees of freedom involved in $\xi$ (forming C−C and breaking C−O bonds), using fixed increments for the bonds (+0.01, 0, −0.01 Å). MC/FEP calculations were employed to compute the free-energy differences ($\Delta G$) between each perturbed state and the reference state. The most negative $\Delta G$ value was then identified, and the reaction coordinate geometry of the most stable state was taken as the new reference geometry. This procedure was repeated until no negative $\Delta G$ values were found, in this manner locating the free-energy minimum with respect to $\xi$ in each environment. To locate the free-energy maximum with respect to $\xi$ in the three media, we performed MC/FEP calculations to map the degrees of freedom involved in $\xi$ near the TS obtained from the gas-phase MERP. Again, bond increments of 0.01 Å were used, and, with the exception of the reaction coordinate $\xi$, the remainder of the system was fully flexible in all calculations. Thus, after determining the true free-energy minimum and maximum in each environment, we corrected the respective 1D pmf results. In this manner, the exact free-energy changes for the conversion of NACs($\xi_{\mathrm{min}}$) into TS, $\Delta G_{\mathrm{NACs}(\xi\mathrm{min})\rightarrow\mathrm{TS}}$ (Figure 1), were obtained. Use of the current QM/MM procedure yields the minimum free-energy reaction path (MFERP) and introduces a significant benefit over previous studies using MERPs in that the reaction path is no longer assumed to be the same in different media. Scheme 2 summarizes the steps employed to obtain $\Delta G_{\mathrm{NACs}(\xi\mathrm{min})\rightarrow\mathrm{TS}}$ in each environment.

***Scheme 2.*** Steps Used To Obtain $\Delta G_{\mathrm{NACs}(\xi\mathrm{min})\rightarrow\mathrm{TS}}$ in Each Environment

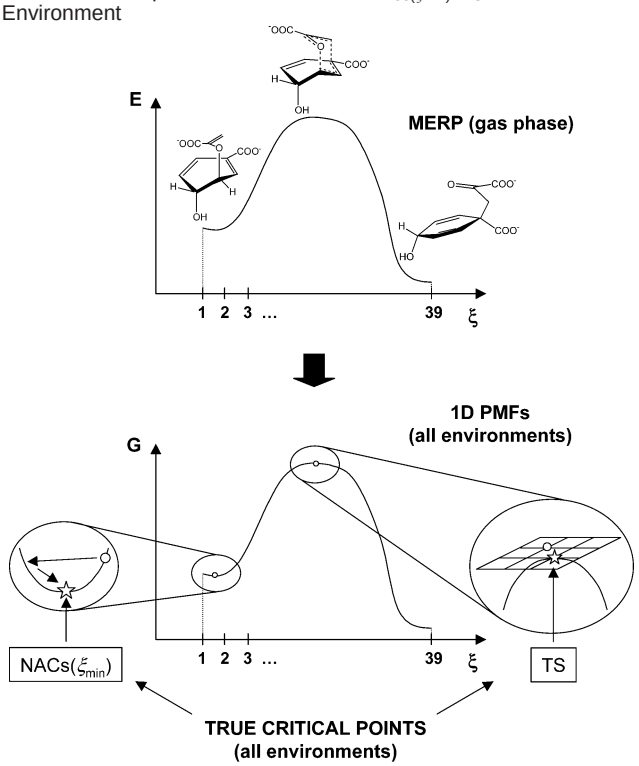


In this work, $\Delta G_{\mathrm{preq}}$ was obtained by computing pmf curves for the reaction coordinate that converts non-NACs into NACs in the gas phase, methanol, and water. The reaction coordinate criterion that differentiates non-NACs from NACs was defined only by the forming C−C bond ($R_{\mathrm{CC}}$). There is clearly some arbitrariness in such definitions.[8,9] Because chorismate is a fairly rigid molecule, we believe that it is not necessary to include an attacking angle for the characterization of the present NACs.[8] Specifically, all conformations that have an $R_{\mathrm{CC}}$ less than or equal to 3.70 Å, a distance shorter than the van der Waals interaction distance between vinyl carbons, have a viable attacking angle, and are characterized as NACs. Thus, pmf curves were computed with respect to $R_{\mathrm{CC}}$, $G(R_{\mathrm{CC}})$, in the gas phase, methanol, and water, using increments of 0.02 Å. The lower limit for $R_{\mathrm{CC}}$ was determined as the value of $R_{\mathrm{CC}}$ in which the ether C−O linkage begins to break to form the transition state. The upper limit for $R_{\mathrm{CC}}$ was determined as the value of $R_{\mathrm{CC}}$ in which the chorismate structure begins to deform from a normal

(15) Blake, J. F.; Jorgensen, W. L. *J. Am. Chem. Soc.* **1991**, *113*, 7430−7432.
(16) Chandrasekhar, J.; Shariffskul, S.; Jorgensen, W. L. *J. Phys. Chem. B* **2002**, *106*, 8078−8085.
(17) Repasky, M. P.; Jorgensen, W. L. *J. Chem. Soc., Faraday Discuss.* **1998**, *110*, 379−389.
(18) Severance, D. L.; Jorgensen, W. L. *J. Am. Chem. Soc.* **1992**, *114*, 10966−10968.
(19) Jones-Hertzog, D. K.; Jorgensen, W. L. *J. Am. Chem. Soc.* **1995**, *117*, 9077−9078.
(20) Dewar, M. J. S., Zoebisch, E. G.; Healy, E. F.; Stewart, J. J. P. *J. Am. Chem. Soc.* **1985**, *107*, 3902−3909.
(21) Stewart, J. J. P. *J. Comput.-Aided Mol. Des.* **1990**, *4*, 1−105.
(22) Gonzalez, C.; Schlegel, H. B. *J. Phys. Chem.* **1990**, *94*, 5523−5532.

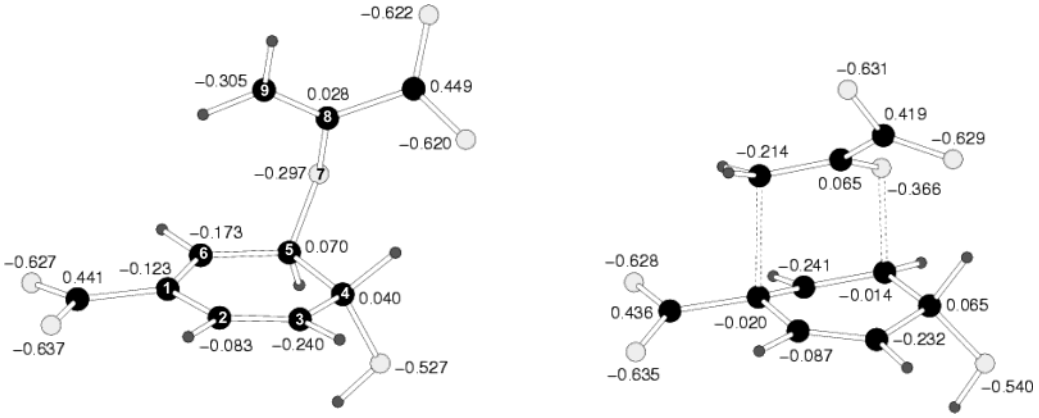


***Figure 2.*** CM1A atomic charges of the heavy atoms for the AM1 reactant and transition state structures.

geometry for a ground state. All pmf curves were zeroed at $R_{CC}$ = 3.668 Å, which is the value for the potential energy minimum of chorismate in the gas phase. The radial distribution function for $R_{CC}$ ($g(R_{CC})$) in each environment was obtained from $G(R_{CC})$. The probability of sampling $R_{CC}$ ($P(R_{CC})$) in the gas phase, methanol, and water was obtained as a product of the respective $g(R_{CC})$ and the volume element of the configuration space corresponding to the coordinate $R_{CC}$. The volume element can be interpreted as a quantity proportional to the probability of sampling $R_{CC}$ with the potential function set to zero.[14] In the present case, the volume element is $4\pi R_{CC}^2$.

To obtain $P_{NACs(\xi min)}$, and consequently $\Delta G_{NACs \rightarrow NACs(\xi min)}$ (see eq 2), it is noted that $P_{NACs(\xi min)}$ may be written as the product of the probability of sampling the $R_{CC}$ distance of NACs($\xi_{min}$) out of all NACs ($P(R_{CC(\xi min)})$), and the probability of sampling the $R_{CO}$ distance of NACs($\xi_{min}$) when $R_{CC}$ is kept fixed with the geometry found in NACs($\xi_{min}$) ($P(R_{CO(\xi min)}|R_{CC(\xi min)})$). Thus, pmf curves were obtained with respect to $R_{CO}$ ($G(R_{CO})$) in the gas phase, methanol, and water, using increments of 0.01 Å, but fixing $R_{CC}$ to its value in NACs($\xi_{min}$) found in each environment. All pmf curves are relative to the gas-phase potential energy minimum $R_{CO}$ distance for chorismate ($R_{CO}$ = 1.431 Å). $P(R_{CC(\xi min)})$ was then multiplied by $P(R_{CO(\xi min)}|R_{CC(\xi min)})$, obtained as a product of the respective $g(R_{CO(\xi min)}|R_{CC(\xi min)})$ and $4\pi R_{CO(\xi min)}^2$, to calculate $P_{NACs(\xi min)}$.

The QM/MM method[23,24] as implemented in BOSS 4.2[25] was used to perform all FEP calculations. Established procedures were employed including Metropolis and preferential sampling, periodic boundary conditions for the solutions, and the Zwanzig equation.[26,27] Statistical uncertainties were obtained from the batch means procedure with batch sizes of $1 \times 10^6$ configurations.[26] In this QM/MM implementation, the solute intramolecular energy is treated quantum mechanically using AM1. Computation of the QM energy and atomic charges are required with every attempted solute move, which occurred every 200 configurations. Intermolecular interactions of the solute with the solvent are given as the sum of all interactions between solute and solvent atoms ($E_{as}$) in eq 3.

$$E_{as} = \sum_{i}^{on\ s} \sum_{j}^{on\ a} [q_i q_j e^2 / r_{ij} + 4\epsilon_{ij}(\sigma_{ij}^{12}/r_{ij}^{12} - \sigma_{ij}^{6}/r_{ij}^{6})] \qquad (3)$$

Partial atomic charges for the solute were obtained from the CM1A procedure,[28] while standard Lennard-Jones parameters were assigned for solute atoms [for C, $\sigma$ = 3.550 Å, $\epsilon$ = 0.070 kcal/mol; for H, $\sigma$ = 2.460 Å, $\epsilon$ = 0.030 kcal/mol; for hydroxyl H, $\sigma = \epsilon = 0.000$; for O, $\sigma$ = 3.000 Å, $\epsilon$ = 0.170 kcal/mol]. The four-site TIP4P[29] and three-site OPLS-UA[30] models were used to describe water and methanol, respectively.

All MC simulations were performed in the NPT ensemble at 25 °C and 1 atm. 825 methanol and 934 water molecules were used, leading to solvent boxes with approximate dimensions of 39 × 39 × 39 Å and 32 × 32 × 32 Å, respectively. Solute−solvent intermolecular cutoff distances of 12 Å were used for both water and methanol, while solvent−solvent cutoffs of 12 Å were employed, based roughly on center-of-mass separations. The intermolecular interactions were quadratically feathered to zero over the last 0.5 Å. To ensure convergence, each MC simulation was extensive. Initial equilibration of the solvent was performed for 500 K configurations, keeping the volume of the system and the solute fixed. Further solvent equilibration entailed $1 \times 10^6$ configurations with only the solute fixed. Finally, $10 \times 10^6$ configurations of additional equilibration prior to $30 \times 10^6$ configurations of averaging were executed for each window in each MC/FEP calculation.

## Results and Discussion

The performance of AM1 must be considered for the chorismate to prephenate rearrangement to assess potential errors that may arise from deficiencies in the semiempirical method. The structures of the potential energy minimum and transition state from AM1 are presented in Figure 2 along with the CM1A charges of the heavy atoms. The reaction is found to occur through a chair transition structure, similar to that found by RHF/6-31G* and BLYP/6-31G* calculations.[31−33] The AM1 transition structure is found to be more compact than ab initio geometries with a forming C−C bond length of 2.120 Å and a breaking C−O bond length of 1.824 Å. This is consistent with a previous study which examined the Claisen rearrangements of allyl vinyl ether and allyl phenyl ether, where AM1 transition structures were found to be significantly tighter with greater 1,4-diyl character than various ab initio structures.[34]

The CM1A charges for the AM1-optimized critical points can be compared to CHELPG charges[35] for the pseudodiaxial

(23) Warshel, A.; Levitt, M. *J. Mol. Biol.* **1976**, *103*, 227−249.
(24) Kaminski, G. A.; Jorgensen, W. L. *J. Phys. Chem. B* **1998**, *102*, 1787−1796.
(25) Jorgensen, W. L. *BOSS*, Version 4.2; Yale University: New Haven, CT, 2000.
(26) Allen, M. P.; Tildesley, D. J. *Computer Simulations of Liquids*; Clarendon Press: Oxford, U.K., 1987.
(27) Zwanzig, R. W. *J. Chem. Phys.* **1954**, *22*, 1420−1426.
(28) Storer, J. W.; Giesen, D. J.; Cramer, C. J.; Truhlar, D. G. *J. Comput.-Aided Mol. Des.* **1995**, *9*, 87−109.
(29) Jorgensen, W. L.; Chandrasekhar, J.; Madura, J. D.; Impey, W.; Klein, M. L. *J. Chem. Phys.* **1983**, *79*, 926−935.
(30) Jorgensen, W. L. *J. Phys. Chem.* **1986**, *90*, 1276−1284.
(31) Davidson, M. M.; Hillier, I. H. *J. Chem. Soc., Perkin Trans. 2* **1994**, 1415−1418.
(32) Wiest, O.; Houk, K. N. *J. Org. Chem.* **1994**, *59*, 7582−7584.
(33) Wiest, O.; Houk, K. N. *J. Am. Chem. Soc.* **1995**, *117*, 11628−11639.
(34) Meyer, M. P.; DelMonte, A. J.; Singleton, D. A. *J. Am. Chem. Soc.* **1999**, *121*, 10865−10874.
(35) Breneman, C. M.; Wiberg, K. B. *J. Comput. Chem.* **1990**, *11*, 361−373.

chorismate conformer and TS previously obtained from RHF/6-31G* geometry optimization.[5] CM1A partial atomic charges are of similar quality, although generally they are less polarized than those from the CHELPG electrostatic potential fitting model using RHF/6-31G* wave functions.[24] The largest change in charge for a hydrogen bond donor/acceptor atom is for the hydroxyl oxygen (0.130 *e* in going from chorismate to the TS) by CHELPG and for the ether oxygen (0.069 *e* in going from chorismate to the TS) by CM1A. The largest variation in CHELPG atomic charges in going from chorismate to the TS was found to be for the ring carbon atom which is involved in the C−C bond forming process, 0.599 *e* by CHELPG and 0.103 *e* by CM1A. Charges for buried atoms are often not well determined with electrostatic fitting procedures.[36] Total charge shifts for the key fragments in going from chorismate to the TS can also be considered. The total CM1A charge for the heavy atoms in the enol pyruvate group for the AM1 TS is −1.356 *e*, while the CHELPG figure for the RHF/6-31G* TS is −1.330 *e*. Similar results are found for chorismate with enol pyruvate charges of −1.367 *e* and −1.360 *e* from CM1A and CHELPG. The total charge difference for heavy atoms in going from chorismate to the TS is 0.011 *e* by CM1A and 0.030 *e* by CHELPG. In view of the simultaneous bond making and breaking, the direction of charge shifts at specific atoms is difficult to predict except that one expects the ether oxygen to become more negative and the pyruvate terminus (C9 in Figure 2) to become more positive in going to the TS. These shifts are reproduced, and, overall, there is nothing unusual in the CM1A charge distributions to cause concern for the present application. In fact, the CM1A charges in Figure 2 are generally similar to OPLS-AA charges for the constituent functional groups,[37] and CM1A charges have performed well in prior studies of solvent effects on equilibria and reactions.[24]

Finally, AM1 gas-phase activation barriers have been found to be larger than those from the best ab initio calculations. The gas-phase enthalpic barrier was found here to be 43.9 kcal/mol from AM1, and the gas-phase free-energy barrier was computed to be 49.2 ± 0.1 kcal/mol (without including $\Delta G_{\mathrm{NACs}\rightarrow\mathrm{NACs}(\xi\mathrm{min})}$, $\Delta G_{\mathrm{preq}}$, and without critical point corrections). Marti and co-workers calculated a $\Delta G^{\ddagger}$ of 48.9 kcal/mol in a QM/MM pmf study using an AM1 quantum component.[38] They suggested subtracting 8.7 kcal/mol from the computed $\Delta G^{\ddagger}$ as a correction to account for the difference between the AM1 and B3LYP/6-31G** enthalpic barriers. Application of their correction term to our calculated gas-phase free-energy barrier leads to a free-energy difference of 40.5 kcal/mol, which is close to the estimated BLYP/6-31G* $\Delta G^{\ddagger}$ barrier of 43.5 kcal/mol.[5] Thus, the free-energy activation barrier in the gas phase with AM1 is too large, and overestimation of the barrier height for the reaction in any medium is inevitable.

However, in comparisons of experimental and calculated $\Delta\Delta G^{\ddagger}$ for different solvents, the energetic deficiencies of AM1 should cancel, and the ability of the present methodology to reproduce the solvent effects can be discerned.

**NACs versus non-NACs.** The results for the NACs/non-NACs equilibria are shown in Figure 3, which displays the pmf

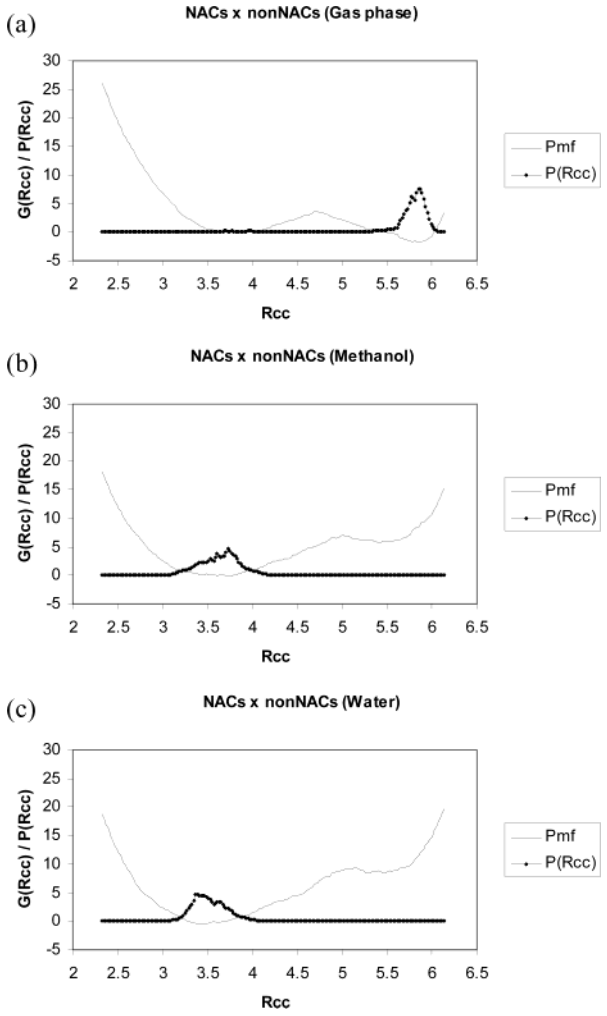


***Figure 3.*** Plots of the one-dimensional potential of mean force for the change in $R_{CC}$ (the forming C−C bond length) and the probability of sampling it in the (a) gas phase, (b) methanol, and (c) water.

curves ($G(R_{CC})$) and the probability of sampling $R_{CC}$ ($P(R_{CC})$) in the gas phase, methanol, and water. As mentioned above, all conformations with $R_{CC}$ less than or equal to 3.70 Å are characterized as NACs. Figure 3a shows that the most stable chorismate conformers in the gas phase have $R_{CC}$ values from ca. 3.6 to 4.1 Å, and from ca. 5.4 to 6.0 Å. However, conformers with $R_{CC}$ values in the latter region are up to 1.7 kcal/mol more stable than those at the shorter separations. This primarily results from formation of an internal hydrogen bond between the hydroxyl group and the enol pyruvate carboxylate. Because of this interaction, the probability of sampling NACs in the gas phase is only 1.3%, while the probability of sampling non-NACs is 98.7%, giving a preequilibrium free energy ($\Delta G_{\mathrm{preq}}$) of 2.6 kcal/mol. Visualization of the most stable NACs in the gas phase reveals that the conformation of the ring is nearly flat. Furthermore, the pseudodiaxial conformation is preferentially represented only when $R_{CC}$ is smaller than ca. 3.1 Å. In view of Figure 3, NACs with the pseudodiaxial conformation are not significantly populated because they are more than 4.7 kcal/mol higher in free energy than the most stable NACs. The most stable non-NACs have pseudodiequatorial conformations to propitiate the formation of the internal hydrogen bond in the gas phase. Some non-NACs do have the pseudodiaxial confor-

(36) Bayly, C. I.; Cieplak, P.; Cornell, W.; Kollman, P. A. *J. Phys. Chem.* **1993**, *97*, 10269−10280.
(37) Jorgensen, W. L.; Maxwell, D. S.; Tirado-Rives, J. *J. Am. Chem. Soc.* **1996**, *118*, 11225−11236.
(38) Marti, S.; Andrés, J.; Moliner, V.; Silla, E.; Tuñón, I.; Bertrán, J.; Field, M. J. *J. Am. Chem. Soc.* **2001**, *123*, 1709−1712.

mation, although they were not observed to be sampled frequently during the pmf calculations.

Figure 3b shows that the most stable chorismate conformers in methanol have $R_{CC}$ values between ca. 3.3 and 3.9 Å, that is, somewhat more compressed than those observed in the gas phase. This is most likely due to enhanced long-range electrostatic interactions with the solvent, when the two carboxylate groups are closer together. As compared to the pmf curve in the gas phase, it is also observed that longer $R_{CC}$ distances are no longer favored in methanol, being ca. 6.0 kcal/mol higher in free energy than the most stable chorismate conformers. Competition with the hydrogen bonding solvent breaks the internal hydrogen bond between the hydroxyl group and the enol pyruvate carboxylate and destabilizes conformers with longer $R_{CC}$. This considerably increases the population of NACs to 56.9% and reduces the population of non-NACs to 43.1%. As a consequence, $\Delta G_{preq}$ in methanol is negative (−0.2 kcal/mol) and does not contribute to $\Delta G^{\ddagger}$. As was observed in the gas phase, the ring conformation for the most stable NACs in methanol is preferentially flat, and NACs with pseudodiaxial conformations, which are preferentially sampled only when $R_{CC}$ is smaller than ca. 3.1 Å, are very rare. More specifically, they are more than 1.4 kcal/mol higher in free energy than the most stable NACs. It is interesting to note that, as compared to the gas-phase pmf, conformers with $R_{CC}$ values smaller than ca. 3.1 Å are not so unstable, again probably due to enhanced long-range electrostatic interactions with the solvent as a result of the proximity of the two carboxylate groups. As in the gas-phase simulations, it was also observed that some of the non-NACs adopt pseudodiaxial conformations. However, because the internal hydrogen bond is absent in methanol, the conformation of the ring for the most stable non-NACs is nearly flat instead of pseudodiequatorial.

Figure 3c shows that the most stable chorismate conformers in water have $R_{CC}$ values between ca. 3.2 and 3.8 Å, which reflects further compression. As compared to the pmf curve in the gas phase, it is again observed that longer $R_{CC}$ distances are no longer significantly populated in water because the corresponding free energies are ca. 8.5 kcal/mol higher than those for the most stable chorismate conformers. Water competes even more effectively than methanol against the internal hydrogen bond between the hydroxyl group and the enol pyruvate carboxylate, and the conformers with longer $R_{CC}$ are further destabilized. Consequently, in water, the population of NACs (81.9%) is the greatest, and the population of non-NACs (18.1%) is the smallest among the three environments. Thus, $\Delta G_{preq}$ in water is also negative (−0.9 kcal/mol) and does not contribute to $\Delta G^{\ddagger}$. Interestingly, in a recent study, Hur and Bruice[39] obtained a very different population of NACs in water, only 0.00007%. This is probably because Hur and Bruice used a force field to describe chorismate, while AM1 was employed in the current study. The ring conformation for the most stable NACs in water is preferentially flat. NACs with pseudodiaxial conformations, which are preferentially sampled when $R_{CC}$ is smaller than ca. 3.1 Å, are more than 1.4 kcal/mol higher in free energy than the most stable NACs. Because the internal hydrogen bonding is also absent in water, the conformation of the ring for the most stable non-NACs is nearly flat instead of pseudodiequatorial. As in the gas-phase and methanol simulations, it was also observed that some of the non-NACs adopt pseudodiaxial conformations.

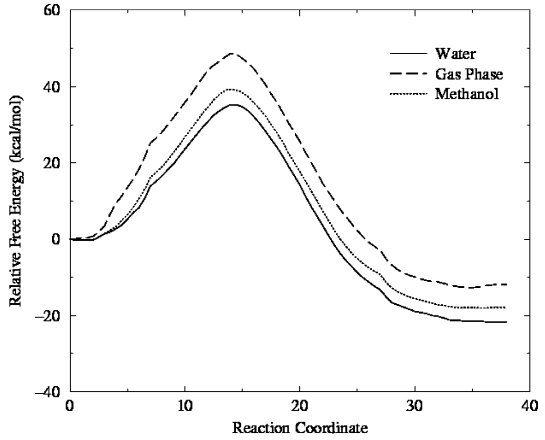


***Figure 4.*** Plots of the one-dimensional potential of mean force in the gas phase, methanol, and water for the chorismate to prephenate rearrangement. The reaction coordinate is the structure number.

As mentioned above, it has been proposed that the 100-fold rate enhancement of the Claisen rearrangement in going from methanol to water ($\Delta\Delta G^{\ddagger} = 3.0$ kcal/mol) arises primarily from shifting the pseudodiequatorial/pseudodiaxial equilibrium.[4,5] However, the present pmf calculations in solution find that both NACs and non-NACs preferentially exhibit a flat ring conformation, and a minor population of each adopts a pseudodiaxial conformation. Thus, the mechanistic view that the pseudodiaxial structure is the reactive conformer capable of progressing to the transition state appears idealized. From the NAC viewpoint, the pseudodiequatorial/pseudodiaxial preequilibrium does not adequately reflect the first step of the reaction. Although the NAC/non-NAC preequilibrium is computed to contribute to $\Delta G^{\ddagger}$ in the gas phase, in water and methanol $\Delta G_{preq}$ is negative and unimportant to the kinetics. Therefore, the 100-fold rate enhancement of the Claisen rearrangement in going from methanol to water is anticipated to arise solely from the free-energy difference associated with the conversion of NACs to the transition state ($\Delta G_{TS}$) in each solvent.

**Pmf's Using the Gas-Phase MERP.** The pmf results for the chorismate to prephenate rearrangement using the gas-phase reaction path are shown in Figure 4. The smooth profiles suggest that the choices of window sizes and the number of configurations sampled were appropriate. The reaction coordinate was followed from the gas-phase geometry for $\xi$ at the potential energy minimum for chorismate, with $R_{CO}$ and $R_{CC}$ distances of 1.431 and 3.668 Å, to the gas-phase minimum energy structure for prephenate. Upon solvation, slightly compressed geometries were obtained for the reactant in these 1D pmf curves. The chorismate structure shifts to $R_{CO}$ and $R_{CC}$ distances of 1.437 and 3.544 Å for methanol and 1.442 and 3.448 Å for water. Formation of these structures is favorable by $-0.2 \pm 0.1$ and $-0.4 \pm 0.1$ kcal/mol, respectively.

The transition states in both solvents were identified in the 1D pmf's as having $R_{CO}$ and $R_{CC}$ bond lengths of 1.824 and 2.120 Å, which show no shift from the transition state structure in the gas-phase MERP. The activation barriers obtained from the 1D pmf's then represent the free energy required in going from the free-energy minimum for chorismate to the TS in the given solvent. For water and methanol, activation barriers of

(39) Hur, S.; Bruice, T. C. *J. Am. Chem. Soc.* **2003**, *125*, 1472−1473.

***Table 1.*** Computed and Experimental Free-Energy Changes for the Claisen Rearrangement of Chorismate[a]

| | gas phase | methanol | water |
|---|---|---|---|
| $\Delta G_{preq}$[b] | 2.6 | −0.2 | −0.9 |
| $\Delta G_{NACs\rightarrow NACs(\xi min)}$[c] | 2.2 | 2.6 | 2.7 |
| $\Delta G_{NACs(\xi min)\rightarrow TS}$ (1D pmf's)[d] | 49.2 ± 0.1 | 39.4 ± 0.2 | 35.6 ± 0.5 |
| $\Delta G_{NACs(\xi min)\rightarrow TS}$[e] | 49.1 ± 0.1 | 39.6 ± 0.2 | 35.4 ± 0.5 |
| $\Delta G_{TS}$[f] | 51.3 ± 0.1 | 42.2 ± 0.2 | 38.1 ± 0.5 |
| $\Delta G_{calc}^{\ddagger}$[g] | 53.9 ± 0.1 | 42.2 ± 0.2 | 38.1 ± 0.5 |
| $\Delta G_{exp}^{\ddagger}$ | n.a. | 27.5[h] | 24.5[h] |
| $\Delta\Delta G_{calc}^{\ddagger}$ | 15.8 ± 0.5 | 4.1 ± 0.5 | 0.0 |
| $\Delta\Delta G_{exp}^{\ddagger}$ | n.a. | 3.0 | 0.0 |

[a] Values in kcal/mol. [b] Obtained by eq 1. [c] Obtained by eq 2. [d] The error in $\Delta G_{NACs(\xi min)\rightarrow TS}$ (1D pmf's) was calculated by propagating the standard deviation ($\sigma_i$) on the individual $\Delta G_i$ used to obtain the pmf curve. The equation $\sqrt{\sum_i^N \sigma_i^2}$ was used, where $N$ is the number of $\Delta G_i$ values. [e] With critical point corrections (see text for details). [f] $\Delta G_{TS} = \Delta G_{NACs\rightarrow NACs(\xi min)} + \Delta G_{NACs(\xi min)\rightarrow TS}$. [g] When $\Delta G_{preq}$ is positive, $\Delta G_{calc}^{\ddagger} = \Delta G_{preq} + \Delta G_{TS}$. When it is negative, $\Delta G_{calc}^{\ddagger} = \Delta G_{TS}$. [h] Reference 4.

35.6 ± 0.5 and 39.4 ± 0.2 kcal/mol are obtained from the 1D pmf curves (Table 1).

**Refinement of Reactant and TS.** To locate the true critical points on the free-energy surfaces, the regions surrounding the free-energy minima and maxima from the 1D pmf's were explored. This was necessary as the 1D reaction coordinate is a composite of $R_{CC}$ and $R_{CO}$, and the true critical points can occur at any $R_{CC}$ and $R_{CO}$ distances. Starting with the gas-phase geometry for $\xi$ at the potential energy minimum for chorismate ($R_{CO}$ = 1.431 Å and $R_{CC}$ = 3.668 Å), we identified the true free-energy minimum (Figure 5). The resultant NACs($\xi_{min}$) have the following geometries: $R_{CO}$ = 1.43 Å and $R_{CC}$ = 3.70 Å in the gas phase, $R_{CO}$ = 1.43 Å and $R_{CC}$ = 3.54 Å in methanol, and $R_{CO}$ = 1.44 Å and $R_{CC}$ = 3.53 Å in water. These geometries are more stable than the starting configuration by 0.07, 0.37, and 0.26 kcal/mol, respectively. Again, slightly compressed geometries in solution were obtained. Comparison of the NACs($\xi_{min}$) to the free-energy minima from the structures in the 1D pmf's, $R_{CO}$ = 1.431 Å and $R_{CC}$ = 3.668 Å in the gas phase, $R_{CO}$ = 1.437 Å and $R_{CC}$ = 3.544 Å in methanol, and $R_{CO}$ = 1.442 Å and $R_{CC}$ = 3.448 Å in water, shows that the 1D pmf's closely identified the true free-energy minimum in all cases. It is notable that all NACs($\xi_{min}$) are indeed NACs, because all have $R_{CC}$ values less than or equal to 3.70 Å. The NACs($\xi_{min}$) $R_{CC}$ distances found in water and methanol closely parallel the most favorable $R_{CC}$ distances found in investigating the relative populations of NACs and non-NACs (Figure 3). The $R_{CO}$ and $R_{CC}$ distances for NACs($\xi_{min}$) are also very similar to the distances from a previous QM/MM pmf study, which yielded average C−O and C−C bond lengths of 1.445 and 3.749 Å for chorismate in water.[38]

To locate the transition state structures, similar free-energy mapping was performed near the maximum in the gas-phase MERP ($R_{CO}$ = 1.824 Å and $R_{CC}$ = 2.120 Å) (Figure 6). As noted above, this geometry did not shift in the 1D pmf calculations. The resultant optimized TS structures have $R_{CO}$ = 1.84 Å and $R_{CC}$ = 2.13 Å in the gas phase, $R_{CO}$ = 1.81 Å and $R_{CC}$ = 2.10 Å in methanol, and $R_{CO}$ = 1.86 Å and $R_{CC}$ = 2.12 Å in water. The corresponding free-energy changes are small; the TS structures in the gas phase and water are more stable than those obtained from the 1D pmf's by 0.20 and 0.06 kcal/mol, respectively, while the TS in methanol is less stable by 0.01 kcal/mol. Comparison to the transition structures

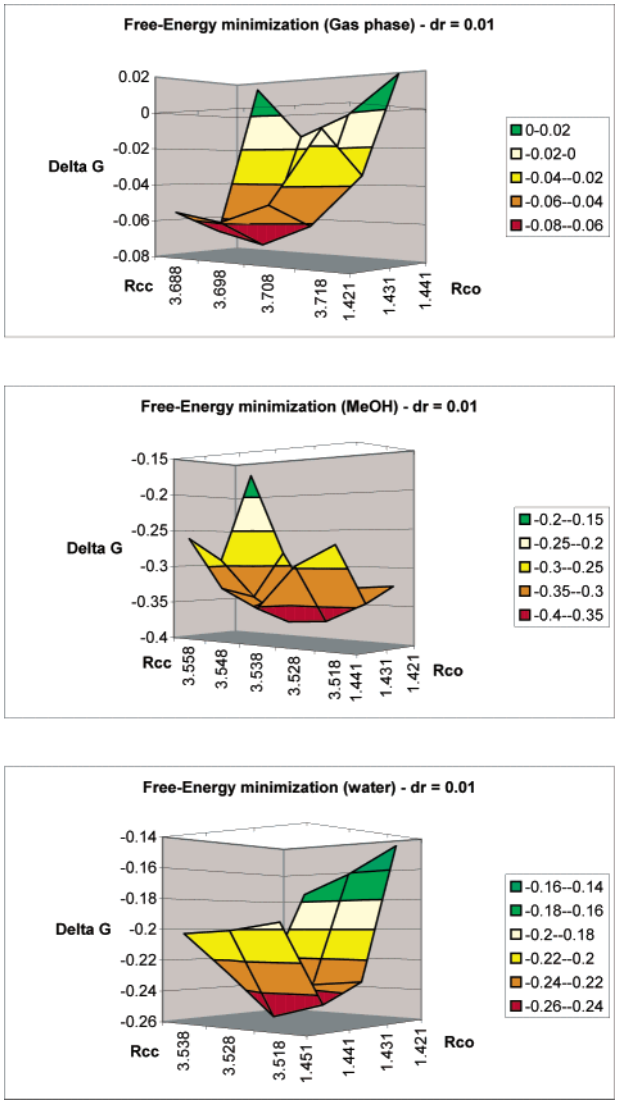


***Figure 5.*** Plots of the two-dimensional potentials of mean force in the gas phase, methanol, and water used to identify the free-energy minimum with respect to $\xi$ in each environment (NACs($\xi_{min}$)).

obtained from the 1D pmf's in all environments, $R_{CO}$ = 1.824 Å and $R_{CC}$ = 2.120 Å, reveals again that the 1D pmf's closely identified the true free-energy critical points; solvent effects play a minor role in the TS structures. In addition, the present TS in water is very similar to that found in the prior QM/MM pmf study, where average C−O and C−C bond lengths of 1.775 and 2.095 Å were reported.[38]

Thus, having determined NACs($\xi_{min}$) and the TS in each environment, we could correct the activation barriers obtained from the 1D pmf's. The results are 49.1 ± 0.1, 39.6 ± 0.2, and 35.4 ± 0.5 kcal/mol for the free energy of conversion of NACs($\xi_{min}$) into the TS, $\Delta G_{NACs(\xi min)\rightarrow TS}$, in the gas phase, methanol, and water, respectively (Table 1). These values are then added to $\Delta G_{NACs\rightarrow NACs(\xi min)}$ to give $\Delta G_{TS}$. Using the pmf calculations described in the Computational Details section, we computed the probabilities of sampling the subset NACs($\xi_{min}$) from all NACs in the gas phase, methanol, and water to be 2.7%, 1.2%, and 1.0%, giving $\Delta G_{NACs\rightarrow NACs(\xi min)}$ values of 2.2, 2.6, and 2.7 kcal/mol, respectively. Thus, the final values of $\Delta G_{TS}$ (Figure 1) in the gas phase, methanol, and water are 51.3 ± 0.1, 42.2 ± 0.2, and 38.1 ± 0.5 kcal/mol (Table 1).

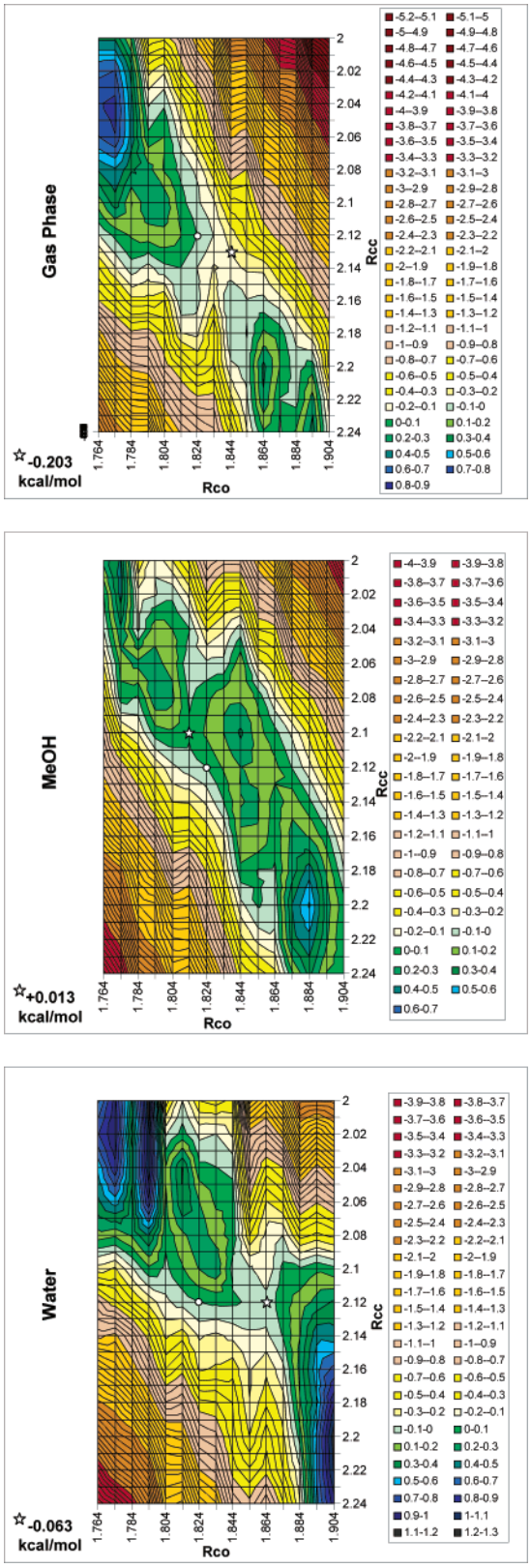


***Figure 6.*** Plots of the two-dimensional potentials of mean force in the gas phase, methanol, and water used to identify the free-energy maximum with respect to $\xi$ in each environment. (○) indicates the TS obtained from the gas-phase MERP calculation and 1D pmf's. (☆) indicates the TS identified by the map.

In the gas phase, $\Delta G_{TS}$ is added to a $\Delta G_{preq}$ of 2.6 kcal/mol, giving a $\Delta G^{\ddagger}$ value of 53.9 ± 0.1 kcal/mol. In the polar protic solvents, $\Delta G_{preq}$ is negative, and $\Delta G_{TS}$ is equal to $\Delta G^{\ddagger}$ in these

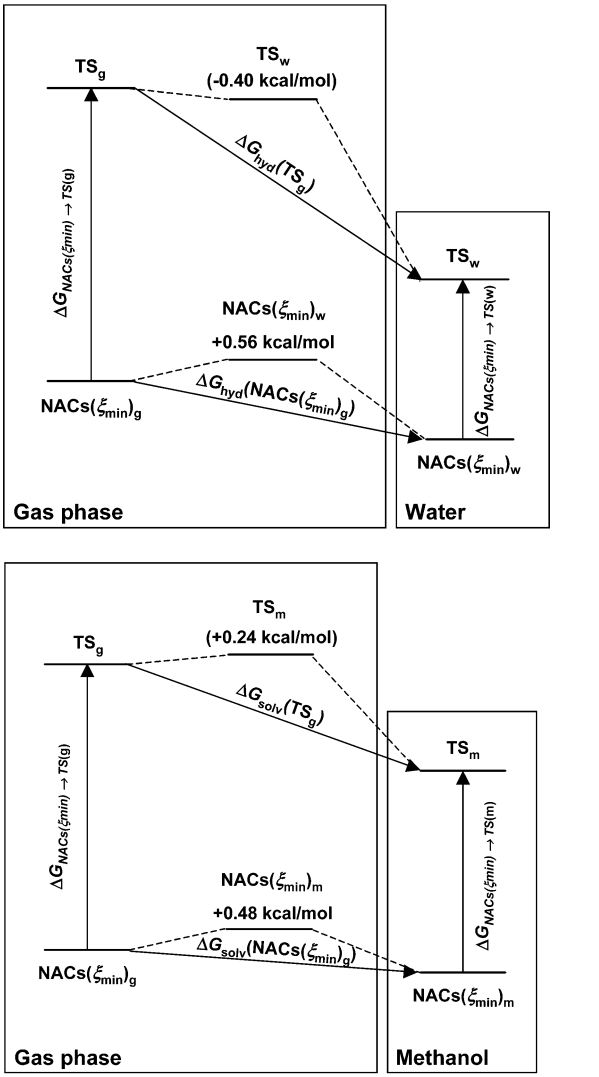


***Figure 7.*** Thermodynamic cycles for the solvation process of NACs$(\xi_{min})_g$ and $TS_g$ in water (top) and in methanol (bottom).

cases. Thus, the absolute theoretical values for $\Delta G^{\ddagger}$ in methanol and water are overestimated with respect to the experimental values, 27.5 and 24.5 kcal/mol.[4,5] However, for the difference in the free energy of activation for the two solvents, $\Delta\Delta G^{\ddagger}$, errors from the semiempirical QM method should largely cancel. Hence, the calculated $\Delta\Delta G^{\ddagger}$ (4.1 kcal/mol) compares well with the experimental value (3.0 kcal/mol). Thus, the present QM/MM MC/FEP method well reproduces the overall rate enhancement in water over methanol, as reflected in Figure 4.

**Solvent Effects on the Claisen Rearrangement.** From the NAC analysis, $\Delta G_{TS}$ is equal to $\Delta G^{\ddagger}$ in the polar protic solvents. Moreover, because the values of $\Delta G_{NACs \rightarrow NACs(\xi min)}$ in methanol and water are very similar, $\Delta\Delta G^{\ddagger}$ between these solvents comes predominantly from $\Delta G_{NACs(\xi min) \rightarrow TS}$ (Figure 1). For an in-depth breakdown of the solvent effects, the thermodynamic cycles shown in Figure 7 can provide a guide. The *vertical arrows* are the free energies associated with the conversion of NACs-($\xi_{min}$) into the TS in the gas phase and in solution. The *diagonal arrows* are the absolute solvation free energies of NACs$(\xi_{min})_g$ and $TS_g$. NACs$(\xi_{min})$ and the TS obtained in methanol and water are then referred to as NACs$(\xi_{min})_m$ and $TS_m$, and NACs$(\xi_{min})_w$ and $TS_w$, respectively. Differences in these quantities will reveal

if the differential solvent effects are dominated by reactant or TS solvation.

The first diagonal *dashed line* in Figure 7 corresponds to the free energy for changing NACs$(\xi_{min})_g$ to NACs$(\xi_{min})_m$ and NACs$(\xi_{min})_w$, and $TS_g$ to $TS_m$ and $TS_w$, all in the gas phase. This defines the intramolecular contributions to solvation, which have been suggested to play a very significant role in the rate enhancement for the Claisen rearrangement occurring in the protein environment,[8,38,40] against the objections of Shurki et al.[13] Using MC/FEP calculations in the gas phase, we computed NACs$(\xi_{min})_w$ to be 0.56 kcal/mol less stable than NACs$(\xi_{min})_g$, and $TS_w$ is 0.40 kcal/mol more stable than $TS_g$. As a consequence, the reaction barrier is around 1.0 kcal/mol smaller in water than in the gas phase because of the intramolecular contributions to solvation. On the other hand, NACs$(\xi_{min})_m$ and $TS_m$ are both less stable than NACs$(\xi_{min})_g$ and $TS_g$ by 0.48 and 0.24 kcal/mol, respectively. Thus, there is only a 0.24 kcal/mol contribution to the rate enhancement in methanol relative to the gas phase because of intramolecular contributions to solvation. Thus, the values for $\Delta\Delta G_{NACs(\xi min)\rightarrow TS}$ between the gas and solution phases are primarily governed, not surprisingly, by the second step of the solvation process.

The second diagonal step is the transfer of NACs$(\xi_{min})$ and the TS from the gas phase to methanol and water (Figure 7). We have not computed these transfer free energies from FEP calculations. However, insights into the differential solvation can be obtained from analyses of the hydrogen bonding for NACs$(\xi_{min})$ and the TS in water and methanol. First, the changes in hydrogen bonding are reflected in solvent−solute energy pair distributions (EPD).[5] The EPD plots obtained from MC simulations with averaging over $30 \times 10^6$ configurations are shown in Figure 8. Standard features are a low-energy band from hydrogen-bonded solvent molecules and a large peak centered at 0 kcal/mol from the many distant molecules with little or no interaction with the solute. Integration of the lowest-energy band from −20.0 to −10.5 kcal/mol for water reveals 12.4 and 13.7 well-bound water molecules for NACs$(\xi_{min})_w$ and $TS_w$, while integration from −20.0 to −9.5 kcal/mol for methanol reveals 9.8 and 9.6 well-bound methanol molecules for NACs$(\xi_{min})_m$ and $TS_m$, respectively. The most attractive solvent−solute interactions represented within this peak can be assigned to the solvent molecules that are hydrogen-bonded to the carboxylate groups. The present numbers of hydrogen bonds per carboxylate group are consistent with the accepted averages in water and methanol of six and five.[5]

Second, specific hydrogen-bond analyses were carried out using geometric criterion for a hydrogen bond, an O- - -HO distance below 2.5 Å and an O- - -HO angle above 120°. The analyses were performed for 250 MC configurations that were saved uniformly during the averaging periods. The changes in the number of hydrogen bonds to the carboxylates in going from NACs$(\xi_{min})$ to the TS in water and methanol were found to be +1.4 and −0.5 molecules, respectively. These values are in accord with the differences from integration of the lowest energy peaks in the EPDs, +1.3 and −0.2 molecules. If the integration limit in methanol is shifted from −9.5 to −10.5 as in water, the difference becomes −0.3 interaction. Additionally, the downward shift in the low-energy band for the EPD in water

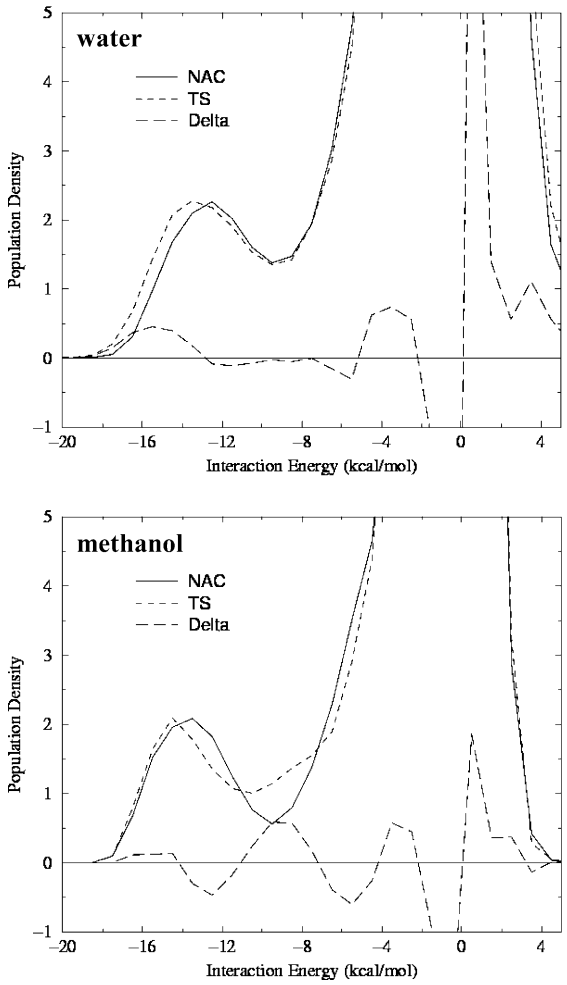


***Figure 8.*** Solvent−solute energy pair distributions (EPD) for NACs$(\xi_{min})$ and the TS in water (top) and in methanol (bottom).

(Figure 8) shows an enhancement of the most favorable interactions in progressing to the TS that is not found in methanol. Thus, the results show an increase in number and strength of the carboxylate-solvent hydrogen bonds in water, while no significant change in carboxylate solvation is found in methanol.

The geometric analyses also confirmed the previously identified increase in the number of hydrogen bonds to the ether oxygen in progressing to the TS for the Claisen rearrangement.[5,18] More specifically, increases of 0.6 and 1.3 hydrogen bonds were obtained in water and methanol, respectively. In addition, hydrogen bonding with the solute's hydroxyl group was found to be unchanged over the course of the reaction in water with three solvent−hydroxyl interactions, while in methanol a loss of 1.5 interactions was observed. Upon expansion of the integration area of the EPD to −5.5 kcal/mol to include the hydroxyl, ether, and second shell solvent interactions, the differences in numbers of interactions between NACs$(\xi_{min})_w$ and $TS_w$, and NACs$(\xi_{min})_m$ and $TS_m$, are 0.8 and 0.0, respectively. Thus, by all measures, $TS_w$ is better hydrated than NACs$(\xi_{min})_w$ by specific strong interactions with water molecules, while in methanol there is little preferential solvation of $TS_m$ over NACs$(\xi_{min})_m$ from solvent−solute interactions from either the first or the second solvation shells.

The predicted rate enhancement in methanol over the gas phase (Table 1) can be explained by increased favorable long-

(40) Khanjin, N. A.; Snyder, J. P.; Menger, F. M. *J. Am. Chem. Soc.* **1999**, *121*, 11831−11846.

range electrostatic interactions, which are contained in the large peaks in the EPDs centered near −3.0 kcal/mol. From the Born equation, having the two carboxylates closer together leads to a decreased $\Delta G_{Born}$ of up to 2 times that of the infinitely separated case.[41] Transition states in both solvents are better solvated with this mechanism. Thus, in water, $TS_w$ experiences both more favorable hydrogen bonding to first shell water molecules and decreased $\Delta G_{Born}$, while in methanol, the solvent effect primarily arises from the decreased $\Delta G_{Born}$. Water, because of its unique combination of small size and hydrogen bonding potential, is better able to respond to changes in the electronic and geometrical structure of solutes than are bulkier hydrogen bonding solvents.

## Conclusions

A general QM/MM approach has been described for obtaining free energies of activation for reactions in solution. The key steps are (1) generation of the minimum energy reaction path in the gas phase, (2) computation of the corresponding free-energy profile by FEP methods in the gas phase and in solution with complete sampling, except for the reaction coordinate, and (3) location of the true free-energy critical points in the gas phase and in solution by additional FEP mapping off the reaction coordinate. The methodology has been applied to the Claisen rearrangement of chorismate to prephenate in conjunction with an analysis based on the near attack conformation (NAC) concept of Bruice and co-workers.[6−10] Although there is some arbitrariness in the definition of a NAC structure, the non-NACs/NACs equilibrium can be argued to have greater relevance for the chorismate to prephenate reaction mechanism than consideration of the pseudodiequatorial/pseudodiaxial equilibrium as a prestep. With the model in Figure 1, the conversion of non-NACs to NACs was found to be favorable in methanol and water, so $\Delta G_{preq}$ does not contribute to the activation barriers. The free-energy changes for the conversion of all NACs to the NACs with the lowest free energy, $\Delta G_{NACs \rightarrow NACs(\xi min)}$, were then computed to be very similar in methanol and water. Thus, the difference in activation barriers for the reaction arises solely from the conversion of NACs($\xi_{min}$) to TS. The experimental $\Delta\Delta G^{\ddagger}$ is well reproduced between water and methanol, suggesting the viability of the present QM/MM model in studying even this highly charged system.

The rate enhancement in water has been identified as arising from enhanced hydrogen bonding to the carboxylates and ether oxygen atom with additional favorable solvation from a large number of long-range interactions in progressing from the reactant to TS. On the other hand, the rate enhancement in methanol arises primarily from favorable long-range interactions. Detailed thermodynamic analyses (Figure 7) also showed that geometrical changes for reactants and TS do not contribute significantly to the differences in reaction rates between the gas phase and solution. This study of the origin of solvent effects for the rearrangement of chorismate to prephenate provides a reference for a similar analysis for the reaction catalyzed by the enzyme chorismate mutase.

**Acknowledgment.** Thanks are extended to Dr. Modesto Orozco for valuable discussions. Gratitude is expressed to the National Science Foundation and National Institutes of Health (GM32136) for support of this research. C.R.W.G. acknowledges CNPq/Brazil (Conselho Nacional de Desenvolvimento Científico e Tecnológico) for a postdoctoral fellowship.

JA021423Z

(41) Rashin, A.; Honig, B. *J. Phys. Chem.* **1985**, *89*, 5588−5593.